ISSN 2347-3487

Full potential linear augmented plane wave calculations of Electronic and Optical properties in ZnO

M.Benkraouda* and N.Amrane
Physics Department
United Arab Emirates University, Al-Ain, P.O. Box: 17551, U.A.E.

Abstract

In this work we present self-consistent calculations for the electronic and optical properties of Zinc oxide. A theoretical investigation of the electronic properties (band structure, density of charge and contour map) and optical properties (refractive index, absorption coefficient, dielectric constants and reflectivity) of Zinc oxide semiconductor ZnO. A full-potential linearized augmented plane-wave (FPLAPW) method was used within the density functional theory (DFT) along with the generalized gradient approximation (GGA96) exchange correlation potential. The results are compared with the experimental data available and some other theoretical work. We found that the GGA approximation yields only a small improvement to the band gap, however, if we allow for a rigid shift of the band structure, the so-called scissor's operator, the optical properties are excellently reproduced.

Keywords

band structure, refractive index, reflectivity

Council for Innovative Research

Peer Review Research Publishing System

Journal: JOURNAL OF ADVANCES IN PHYSICS

Vol. 11, No. 5

www.cirjap.com, japeditor@gmail.com

ISSN 2347-3487

1-INTRODUCTION

ZnO films have a unique position among materials because they are piezoelectric materials that have been the subject of extensive studies [1–4]. Its piezoelectric properties are exploited in thin films applications, as a surface acoustic wave (SAW) devices, ultrasonic transducers and sensors [5–7]. The crystal structure of ZnO is hexagonal (wurtzite type) which makes it suitable for fabrication of high quality oriented or epitaxial thin film. Each Zn atom is tetrahedrally coordinated with four O atoms and the zinc d electrons hybridize with the oxygen p electrons [8].

ZnO is one of the most important materials for the next generation UV-devices, such as transparent electrode and UV-laser diode. It has a direct band gap of 3.3 eV and exhibits strong room temperature excitonic luminescence as a result of its large exciton binding energy of 60 meV [9,10] Accurate knowledge of the absorption coefficient, optical bandgap and refractive index of semiconductors is essential for the design and analysis of various optical and optoelectronic devices. ZnO films were fabricated with different deposition techniques [11–13], but high-quality films prepared at low temperatures are particularly required in the film technology. In the last years, chemical bath deposition (CBD) has emerged as an interesting method for the deposition of polycrystalline thin film semiconductors, being a low temperature method and also not highly expensive [14, 15].

However, ZnO crystals are a non-stoichiometric material due to the existence of various defects and it has been difficult to obtain stable p-type crystals. While light-emitting diode based on ZnO was successfully reported [16], the control of defects in ZnO is still an important problem for the optoelectronic applications [17]. In our study, we have investigated electronic and optical properties by means of first-principles density-functional total-energy calculation using the all-electron full potential linear augmented plane-wave method (FPLAPW). The equilibrium lattice constants and the bulk moduli (a, c, B and B$'$) are compared with others theoretical and experimental calculations.

2- CALCULATIONS

Scalar relativistic calculations have been performed using the wien2k code [18, 19]. For the exchange correlation potential, we have used the local density approximation (LDA) with a parameterization of Ceperly-Adler data [20]. The new Full Potential Augmented Plane Wave method of the density functional theory is applied [21, 22]. Several improvements to solve the energy dependence of the basis set were tried but the first really successful one was the linearization scheme introduced by Andersen [23] leading to the linearized augmented plane wave (LAPW) method. In LAPW, the energy dependence of each radial wave function inside the atomic sphere is linearized by taking a linear combination of a solution u at a fixed linearization energy and its energy derivative $\dot{u}$ computed at the same energy.

$$\Phi_K(\mathbf{r}) = \begin{cases} \sum_L \left[a_L^{\alpha \mathbf{K}} u_l^{\alpha}(r') + b_L^{\alpha \mathbf{K}} \dot{u}_l^{\alpha}(r') \right] Y_L(\hat{r}') & r' \langle R_\alpha \\ \Omega^{-1/2} \exp\left(i(k+K).r\right) & r \in I \end{cases} \quad (1)$$

Where r'=r-r_α is the position inside sphere α with polar coordinates r' and r, **k** is a wave vector in the irreducible Brillouin zone, **K** is a reciprocal lattice vector and u_l^{α} is the numerical solution to the radial Schrodinger equation at the energy ε. The coefficients $a_L^{\alpha K}$ are chosen such that the atomic functions for all L components match (in value) the PW with K at the Muffin tin sphere boundary. The KS orbitals are expressed as a linear combinations of APWs $\Phi_K(r)$. In 1991 Singh [24] introduced the concept of local orbitals (LOs) which allow an efficient treatment of the semi-core states. An LO is constructed by the LAPW radial functions u and $\dot{u}$ at one energy ε_1 in the valence band region and a third radial function at ε_2.

$$\Phi_{LO}(\mathbf{r}) = \begin{cases} \left[a_L^{\alpha,LO} u_{1l}^{\alpha}(\mathbf{r}') + b_L^{\alpha,LO} \dot{u}_{1l}^{\varepsilon}(\mathbf{r}') + c_L^{\alpha,LO} u_{2l}^{\alpha}(\mathbf{r}') \right] Y_L(\hat{r}') & r' \langle R_\alpha \\ 0 & r \in I \end{cases} \quad (2)$$

Recently, an alternative approach was proposed by Sjöstedt et al [25], namely the APLW+ lo (local orbital) method. Here the augmentation is similar to the original APW scheme but each radial wavefunction is computed at a fixed linearization energy to avoid the non-linear eigenvalue problem. The missing variational freedom of the radial wavefunctions can be recovered by adding another type of local orbitals (termed in lower case to distinguish them from LO) containing u and $\dot{u}$ term:

$$\Phi_{lo}(\mathbf{r}) = \begin{cases} \left[a_L^{\alpha,lo} u_l^{\alpha}(\mathbf{r}') + b_L^{\alpha,lo} \dot{u}_l^{\alpha}(\mathbf{r}') \right] Y_L(\mathbf{r}') & r' \langle R_\alpha \\ 0 & r \in I \end{cases} \quad (3)$$

It was demonstrated that this new scheme converges faster than LAPW. The APW +lo scheme has been implemented in the wien2k code version [26].

More importantly, Generalized gradient approximations (GGA's) for the exchange-correlation energy has also been incorporated; although the GW approximation is a widely used method to predict quasi particle band gaps, as opposed to density functional theory (DFT), which is only applicable to ground state properties, the large computational effort associated with this method limits GW calculations to rather small systems, , one has to note also that GW and hybrid functional can result in band gap error on the order of 10–20% compared to experimental data [27]. There are some other interesting techniques such as the time dependent density functional theory (TDDFT) [28], this method has achieved an unprecedented balance between accuracy and efficiency for calculations of the excitation spectra and response of atoms and molecules, given its simplicity, and the relatively modest CPU cost of this type of calculation. The use of TDDFT is increasing, and it is fast becoming one of the tools of choice to get accurate and reliable predictions for excited-state properties in solid state physics, and chemistry, both in the linear and non-linear regimes.

However, in this article we concentrated on the most common approximation, the GGA which makes non-self-consistent evaluation of the quasi particle self -energy, usually the local-density approximation (LDA) or generalized gradient approximation (GGA) [29], the GGA calculations are performed using a consistent GGA treatment of valence and core electrons.

As the LDA approximates the energy of the true density by the energy of a local constant density, it fails in situations where the density undergoes rapid changes such as in molecules. An improvement to this can be made by considering the gradient of the electron density, the so-called Generalized Gradient Approximation (GGA). Symbolically this can be written as

$$E_{xc} = E_{xc}\left[\rho(r), \nabla\rho(r)\right] \tag{4}$$

there are several different parameterizations of the GGA. A commonly used functional is the PW91 functional, due to Perdew and Yang [30].

However, in the calculations reported here, we chose the muffin tin radii for Zn and O to be 2.0 and 1.9 a.u. respectively. The expansion of the spherical region is developed up to l_{max}=10, while in the interstitial region we have used 2420 plane waves for ZnO. Furthermore, we have used the energy cutoff of $R_{\square\square}.K_{\square\square\square}$=8 and the maximal reciprocal vector equal to 10. The integrals over the Brillouin zone are performed using the Monkorst-pack special k-points approach [31]. Since calculations of the optical properties require a more dense k-matrix, we have used 1000 k-points in the irreducible Brillouin zone for integration in reciprocal space.

Optical properties of a solid are usually described in terms of the complex dielectric function $\varepsilon(\omega) = \varepsilon_1(\omega) + i\varepsilon_2(\omega)$. The dielectric function is determined mainly by the transition between the valence and conduction bands according to perturbation theory, the imaginary part of the dielectric function in the long wavelength limit has been obtained directly from the electronic structure calculation, using the joint density of states (DOS) and the optical matrix elements. It is expressed as

$$\varepsilon_2(\omega) = \frac{4\pi^2 e^2}{3m^2\omega^2} \sum_{l,n} \int_{BZ} \frac{2}{(2\pi)^3} d^3k \left|P_{nl}\right|^2 .\delta\left[E_l(k) - E_n(k) - \hbar\omega\right] \tag{5}$$

Where m is the mass and e the electrical charge of the electron, $\sum_{l,n}$ means the summation between all the conduction bands (l) and valence bands (n); and P_{nl} expresses the momentum matrix element between l and n. It is given by

$$P_{nl} = \frac{m}{\hbar}\left\langle nk\left|\nabla_k H,(k)\right|lk\right\rangle \tag{6}$$

Where H(k) is the Hamiltonian, and $\left\langle nk\right|,\left|lk\right\rangle$ are the k-space wavefunctions. Using the FP-LAPW parameters, we can directly calculate P_{nl}.

The real part of the dielectric function can be derived from the imaginary part by the Kramers-Kronig relationship. The knowledge of both the real and the imaginary parts of the dielectric allows the calculation of important optical functions. In this paper, we also present and analyze the refractive index $n(\omega)$ given by

$$n(\omega) = \left[\frac{\varepsilon_1(\omega)}{2} + \frac{\sqrt{\varepsilon_1^2(\omega) + \varepsilon_2^2(\omega)}}{2}\right]^{1/2} \tag{7}$$

At low frequency (ω=0), we get the following relation:

ISSN 2347-3487

$$n(0) = \varepsilon^{1/2}(0)$$

To correct the LDA error in the band gaps a constant potential was applied to the conduction band states (using the scissors operator which rigidly shifts the conduction band states) in order to match the calculated band gaps with the experimental data.

3. RESULTS

The structural optimization of the wurtzite phase was performed by calculating the total energy as function of the variables c/a and V. The two-dimensional minimization of the total energy versus c/a for a fixed volume requires that each of the self-consistent calculations is converged, so the iteration process was repeated until the calculated total energy of the crystal converged to less than 1 mRyd. A total of seven iterations was necessary to achieve self-consistency. The equilibrium lattice constants and bulk modulus are calculated by fitting the total energy versus volume according to Murnaghan's equation of state [32]. The variation of total energy as a function of volume and c/a is shown in figures 1a and 1b.

The results are also shown along with other theoretical values in Tables 4 and 5. It is found that the generalized gradient approximation (GGA) gives quite nice values comparing to those obtained by other authors.

3.1 Electronic properties

3.1.1 Electronic band structures

Electrons interact with the crystal, and this must express itself in their energies, there is an energy gap in the E = E(k) relation for all k vectors ending on a Brillouin zone.

A general relation yields for the energies of the k_{BZ} electron waves

$$E(k_{BZ}) = \frac{(\hbar k)^2}{2m} \pm |U(g)| \qquad (8)$$

With U(g) being the Fourier component of the periodic potential for the reciprocal lattice vector g considered. The band gap represents the minimum energy difference between the top of the valence band and the bottom of the conduction band.

The electronic band structures of ZnO along symmetry lines is shown in figure 2. The calculated band energy gap at high symmetry points is given in table 1, the bandgap is found to be direct and equal to 1 eV, which is in close agreement with other theoretical calculations as shown in table 1.

It is interesting to note that quasi-particle excitations are not taken into account in density functional theory (DFT), the energy gap calculated from DFT tends to be smaller than the experimental one. There are several reasons for this. One is that the LDA and GGA functionals contain the self-interaction error and do not show a derivative discontinuity, which is important when one wants to compare the Kohn Sham band gap with the experimental band gap. In some cases, the wrong ground state is found, as, e.g., in Ge, where the band gap is around 0.7 eV, whereas the LDA Kohn-Sham gap is slightly negative at ambient pressure [33]. The GGA approximation yields only a small improvement. Quasiparticle calculations essentially overcome the underestimate of the band gap as obtained using the LDA. The GW calculations for GaN for instance predict band structures in much better agreement with experiment; but they are time consuming, and also they treat the d valence states as part of the pseudopotential core in the case of GaN. However, Fig. 2 indicates that ZnO with wurtzite structure has a direct band gap between the top of the valence band and the bottom of the conduction band at the Γ point. The energy levels for the lower part of the valence band vary slowly and are attributed to the semi-core-like Zn 3d states. The upper valence bands are mainly due to the O 2p orbitals and are much flatter as compared with the conduction bands, resulting in heavier effective masses for the valence band holes. This is one of the reasons for the difficulty in manufacturing ZnO.

Table 1. Band energies (eV) for wurtzite ZnO

	Present work	Other calculations	Experiment
Energy gap (eV)	1.0 (GGA96)	0.95 eV (FP-LMTO)[a]	3.22[b]

[a] Reference [34]

[b] Reference [35]

3.1.2 Total charge density

To visualize the nature of the bond character and to explain the charge transfer and the bonding properties of w-ZnO, we calculate the total charge density.

The electronic charge density is obtained for each band n by summing over the k-states in the band.

$$\rho_{n}(\boldsymbol{r}) = \sum_{\boldsymbol{k}} \left|\Psi_{\boldsymbol{nk}}(\boldsymbol{r})\right|^{2} \quad (9)$$

And the total charge density is obtained by summing over the occupied band.

$$\rho_{\boldsymbol{nk}}(\boldsymbol{r}) = \sum_{\boldsymbol{n}} \rho_{\boldsymbol{n}}(\boldsymbol{r}) \quad (10)$$

The total valence charge densities for the three binary compound ZnO is displayed along the Zn-O bonds (Figures 3a and 3b).

Figure 3b shows the charge density distribution in the (110) plane (contour maps). The calculated electron charge distributions indicate that there is a strong ionic character for w-ZnO compounds as can be seen along the Zn-O bonds. The charge densities around the atoms have asymmetric forms which are similar to those given in previous reports using the ab initio pseudopotential method. The charge transfer gives rise to the ionic character in Zinc oxide. The driving force behind the displacement of the bonding charge is the greater ability of Zn to attract electrons towards it due to the difference in the electronegativity of Zn and O.

3.2 Optical properties

The study of the optical constants and their variation with frequency is very interesting for the uses of films in optical applications. These applications require accurate knowledge of the optical constants over a wide wavelength range. Extinction coefficient and refractive index. The reflectivity (R) of materials of refractive index (n) and extinction coefficient (k) is given by:

$$R = \frac{(n-1)^2 + k}{(n+1)^2 - k} \quad (11)$$

Tauc et al. [36] and Davis and Mott [37] gave an equation derived independently for the determination of energy band gap nature and the value of Eg (the energy gap) as

$$\alpha(h\nu) = \frac{c}{h\nu}(h\nu - E_g)^m \quad (12)$$

Where m =1/2 for allowed direct transition, m =3/2 for direct ‘‘forbidden’’ transition, m =2 for allowed indirect transition and m =3 for indirect ‘‘forbidden’’ transition. C is a constant nearly independent on photon energy and known as the disorder parameter. Eg is closely related to energy band gap. Thus, the values of the optical band gap of ZnO films are obtained by plotting $(\alpha h\nu)^{1/2}$ versus $h\nu$ in the high absorption range followed by extrapolating the linear region of the plots to $(\alpha h\nu)^{1/2}$ =0. The analysis of our data showed that plots of $(\alpha h\nu)^{1/2}$ against $h\nu$ give one linear relation which is best fitted by Eq. (9) with m =1/2. This indicates that the allowed direct transition is responsible for interband transition in ZnO binary compound.

The plot of $(\alpha h\nu)^2$ against photon energy for ZnO films is represented in Fig.4 and, as expected from Eq. (9), these are linear at the higher values of $\alpha(h\nu)$ but tend to deviate from linearity at low photon energies. These graphs extrapolated to $h\nu$ axis give the value of Eg .The obtained values of the optical gap Eg is found to be ~ 2.4 eV (Figure 4).

ISSN 2347-3487

We now turn to the analysis of the optical spectra. The dielectric functions of ZnO in the wurtzite structure are resolved into two components $\varepsilon_{xy}(\omega)$, average of the spectra for the polarization along the x and y-directions and ε_Z, the polarization parallel to the z-direction. The calculated dielectric constants are shown in table 2.

Figure 5a shows the variation of the imaginary of the electronic dielectric function for ZnO, for radiation up to 30 eV. The calculated results are rigidly shifted upwards by 1.50 eV. The main feature is a broad peak with a maximum around 10 eV and the maximum amplitude is at 3, a shoulder is also visible at around 4.9 eV. The peak as well as the shoulder are excellently reproduced in the calculations, as are the general form of some experimental spectra. There are also two other groups of peaks, in (11.2 eV- 14.3 eV) photon energy range, they are mainly due to transitions in the vicinity of M. this is usually associated with E_1 transition.

Next, we consider the dispersive part of the dielectric function, ε_1, see figure 5b. The calculated spectra have been obtained by Kramers-Kronig transformation of the shifted ε_2 spectra. The main features are a shoulder at lower energies, a rather steep decrease between 3 and 8 eV, after which ε_1 becomes negative, a minimum and a slow increase toward zero at higher energies. The calculated dielectric constants compared with the experimental data and some other work are shown in table 2.

Table 2: The calculated dielectric constants

	$\varepsilon_{//}$	ε ?
Present work	3.64	3.56
Other work	3.75[a]	3.70[a]
Experiment	3.72[b]	3.68[b]

[a]reference [38]

[b]reference [39]

We now shortly discuss the spectra obtainable from the dielectric function. As seen in figures 6, the refractive index was computed using both real and imaginary parts of the dielectric function. It shows that the refractive index exhibits a significant dispersion in the short wavelength region below λ= 290nm (3.15 eV) where absorption is strong. It decreases with the increase of the energy of the incident light, becoming nearly flat in the higher region. It is observed also that n reached a peak value at 2.55 eV and this peak occurred more or less at the same energy in the real part of the dielectric constant energy dependence curves.

We have fitted our calculated refractive index using the empirical formula of Peng and Piprek [40], given by the following relation:

$$n(E) = \left[a\left(\frac{E}{E_g}\right)^2 \left(2 - \left(1+\frac{E}{E_g}\right)^{0.5} - \left(1-\frac{E}{E_g}\right)^{0.5} \right) + b \right]^{0.5} \qquad (13)$$

Where the values of the direct energy gaps (E_g) are obtained from our optical spectra, and E is the photon energy. The parameters a and b are obtained from the fit of the calculated refractive index spectra for ZnO. All parameters are listed in table 3.

Finally, Figure 7 shows reflectivity spectra, the spectrum is typical for a semiconductor with a high-reflectivity region (R ~ 90% for ω < 5000 cm−1), the reflectivity spectrum spans from about 4eV to 20 eV and correlates very well with the highest reflectivity of ZnO.

Conclusion

The electronic and optical properties of wurtzite ZnO have been investigated using the wien2k package, full-potential linearized augmented plane wave (FP-LAPW) approach within the density functional theory (DFT) in the local spin density approximation (LSDA) including the generalized gradient approximation (GGA) was used. The use of GGA for the exchange-correlation potential permitted us to obtain good structural parameters. The calculated band-gap was also in good agreement with the other theoretical calculations. The real and imaginary parts of the dielectric functions were calculated for polarization in the x,y plane and along the z-axis, the optical properties are excellently reproduced using the density functional theory, if we allow for a rigid shift of the band structure, the so-called scissors operator.

Table 3: The Parameters of Peng and Piprek in ZnO

	E_g (eV)	a	b
ZnO	2.3eV*	3.60	8.74

*As calculated using the scissors operator.

Table 4: Reported and calculated lattice parameters for ZnO.

Lattice parameters	a(Å)	c(Å)
Experiment[b]	3.212[a]	5.228[a]
calculated	3.238	5.205
Deviation	0.026	0.023

[a]Reference [41]

Table 5:

Static equilibrium constant a (Å), bulk modulus B (Mbar), first pressure derivative of the bulk modulus B' for ZnO. Comparison of present results with previous calculations

	Present work	Other calculations	Experiment
Lattice parameters (a-c) (Å)	3.238 –5.205	3.249- 5.206[c]	3.212- 5.228[b]
Bulk modulus (B) (GPa)	161.1	183[a]	142.6[d]
Derivative of bulk modulus (B')	3.866	3.78[e]	3.82[d]

[a]Reference [42]

[b]Reference [41]

[c]Reference [43]

[d]Reference [44]

[e]Reference [45]

Figure captions

Figure 1a: Energy (eV) versus Volume (Å^3)

Figure 1b: Energy (eV) versus (c/a)

Figure 2: Energy (eV) versus Wave vector

Figure 3a: Electron density (arb. Units) versus Position (Atomic units)

Figure 3b: Electron density (arb. Units) versus Position (Atomic units)

Figure 4: Absorption coefficient (α^2) versus Energy (eV).

Figure 5a: Imaginary part of dielectric function versus Energy (eV).

Figure 5b: Real part of dielectric function versus Energy (eV).

Figure 6: Refractive index (n) versus Energy (eV).

Figure 7: Reflectance (R) versus Energy (eV).

REFERENCES

[1] S. Sundar Pareek, K. Pareek, Journal of Applied Physics (IOSR-JAP) 2278-4861, Vol. 3, Issue 2 (2013), PP 16-24

[2] A. Catellani, Alice Ruini, G. Cicero and A. Calzolari, physica status solidi (b) Vol. 250 Issue 10 (2013)

[3] A. Janotti and C. G Van de Walle, Rep. Prog. Phys. 72 (2009) 126501

[4] G. Malloci, L. Chiodo, A. Rubio, A. Mattoni, Journal Of Physical Chemistry C 116, 8741-8746 (2012)

[5] Yanagitani T., Morisato N, Takayanagi S, Matsukawa M, Watanabe Y., IEEE Trans Ultrason Ferroelectr Freq Control. (2011),1062-8

[6] Zhe Wang , Qing-Tang Xue , Yuan-Quan Chen , Yi Shu , He Tian , Yi Yang , Dan Xie, Jian-Wen Luo and Tian-Ling Ren, Sensors (2015), 15, 2538-2547

[7] Weipeng Xuan, Mei He, Nan Meng, Xingli He, Wenbo Wang, Jinkai Chen, Tianjin Shi, Tawfique Hasan, Zhen Xu, Yang Xu & J. K. Luo, Scientific Reports 4, Article number: 7206 (2014)

[8] M. K. Mishra, A. Narayan, R. K. Singh, R. Singh Yadav, N. K. Nidhi, and A. C. Pandey, Indian Journal of Materials Science, Vol. 2013 (2013), Article ID 405147, 6 pages

[9] Agnieszka Kołodziejczak-Radzimska * and Teofil Jesionowski, Materials (2014), 7, 2833-2881; doi:10.3390/ma7042833

[10] Marc Dvorak, Su-Huai Wei and Zhigang Wu, PRL 110, 016402 (2013)

[11] A. Ashour, , M.A. Kaid, N.Z. El-Sayed, A.A. Ibrahim, Volume 252, Issue 22, 15 September (2006), 7844–7848

[12] O. Berestok, D.I. Kurbatov, N.M. Opanasyuk1, A.D. Pogrebnjak, O.P. Manzhos1, S.M. Danilchenko, JOURNAL OF NANO- AND ELECTRONIC PHYSICS , Vol. 5 No 1, 01009, (2013)

[13] Dewei Chu, Sean Li, New Journal of Glass and Ceramics, (2012), 2, 13-16

[14] Nasser Saadaldina, M.N. Alslouma, N. Hussainb, Energy Procedia, Volume 74, August (2015), Pages 1459–1465

[15] P. Gogoi, R. Saikia, D. Saikia, R. P. Dutta and S. Changmai, physica status solidi (a), Vol. 212, Issue 4, 826–830, (2015)

[16] S.J Pearton1, F. Ren ,Current Opinion in Chemical Engineering, Volume 3, February 2014, Pages 51–55

[17] Xinyu Zhang, Jiaqian Qin, Yanan Xue, Pengfei Yu, Bing Zhang, Limin Wang & Riping Liu, Scientific Reports 4, Article number: 4596 (2014)

[18] S. J. Ahmed, J. Kivinen, B. Zaporzan, L. Curiel, S. Pichardo, and O. Rubel, Comp. Phys. Commun. 184, 647-651 (2013)

[19] A. Shankar, D.P. Rai, R. Khenata, J. Maibam, Sandeep, R.K. Thapa, Journal of Alloys and Compounds, 619, (2015), 621-626

[20] S. Boucetta , Journal of Magnesium and Alloys, Volume 2, Issue 1, March 2014, Pages 59–63

[21] Lin-Hui Ye, Phys. Rev. B 91, 075101 – (2015)

[22] Naoyuki Nagasako, and Tamio Oguchi, J. Phys. Soc. Jpn. 82, 044701 (2013)

[23] O.K.Andersen, Phys.Rev.B12 (1975) 3060-3083

[24] D.Singh, Phys.Rev.B 43 (1991) 6388-6392

[25] E.Sjöstedt, L.Nordström, D.J.Singh, Solid State Comm.114 (2000) 15-20

[26] M. Gajdoš, K. Hummer, and G. Kresse, PHYSICAL REVIEW B 73, 045112 (2006)

[27] Fabien Bruneval and Matteo Gatti, Top Curr Chem (2014), DOI: 10.1007/128_2013_460 [28] Sean A. Fischer, Christopher J. Cramer, and Niranjan Govind, J. Chem. Theory Comput., 2015, 11 (9), pp 4294–4303

[29] Javier Carmona-Espíndola, José L. Gázquez, Alberto Vela and S. B. Trickey ,J. Chem. Phys. 142, 054105 (2015)

[30] J. P. Perdew, J. A. Chevary, S. Vosko, K. A. Jackson, M. R. Pederson, D. J. Singh, and C. Fiolhais Phys. Rev. B 46, 6671 (1992)

[31] H.J.Monkhorst, J.D.Pack, Phys.Rev.B13 (1976) 5188

[32] Murnaghan F D 1944 Proc. Natl Acad. Sci. USA 30 5390

[33] M.Alouani and J.M.Wills, Phys.Rev.B54, 2480 (1996)

[34] Sun Yuming, Xu Pengshou, Shi Chaoshu, Xu Faqiang, Pan Haibin and Lu Erdong

Journal of Electron Spectroscopy and Related Phenomena

Volumes 114-116, (2001) 1123-1125.

[35] B.J. Lokhandea, P.S. Patila, M.D, Uplane Physica B 302–303 (2001) 59–63

[36] J. Tauc, R. Grigorovici, A. Vancu, Phys. Stat. Sol. 15

(1966) 627

[37] N.F. Mott, E.A. Davis, Electronic Processes in Non-

Crystalline Materials, Clarendon Press, Oxford, 1979.

[38] Ashkenov N, Mbenkum BN, Bundesmann C, Riede V, Lorenz M, Spemann D, Kaidashev EM, Kasic A, Schubert M, Grundmann M, Wagner G, Neumann H, Darakchieva V, Arwin H, Monemar B. Journal of Applied Physics, 93 no.1 (2003) 126.

[39] Yoshikawa H, Adachi S. Japanese Journal of Applied Physics Part 1-Regular Papers Short Notes & Review Papers, 36 no.10 (1997) 6237.

[40] T.Peng and J.Piprek, Electro. Lett. 32,24 (1996).

[41] A. Abu EL-Fadl_, Galal A. Mohamad, A.B. Abd El-Moiz, M. Rashad Physica B 366 (2005) 44–54

[42] Karzel H, Potzel W, Kofferlein M, Schiessl W, Steiner M, Hiler U, Kalvius GM, Mitchell DW, Das TP, Blaha P, Schwarz K, Pastemak MP. Physical Review B-Condensed Matter 53 no.17 (1996) 11425

[43] **Y**u Chen, Runzhou Yu, Qian Shi, Jingli Qin and Feng Zheng Materials Letters Volume 61, Issue 22, September 2007, Pages 4438-4441.

[44] Desgreniers S. Physical Review B-Condensed Matter 58 no.21 (1998) 14102.

[45] Xiaowei Sun, Zijiang Liub, Qifeng Chenc, Yandong Chua and Chengwei Wangd, Physics Letters A, Volume 360, Issue 2, 25 (2006), Pages 362-366

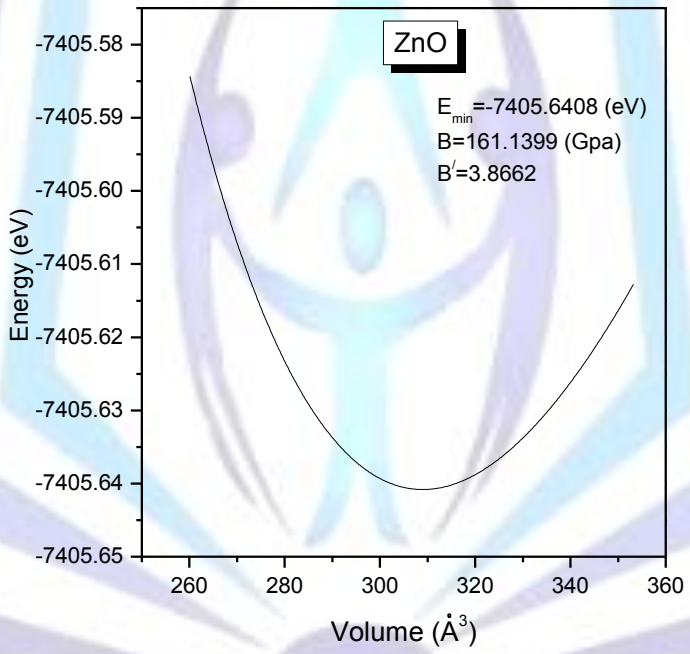

Figure 1a

ISSN 2347-3487

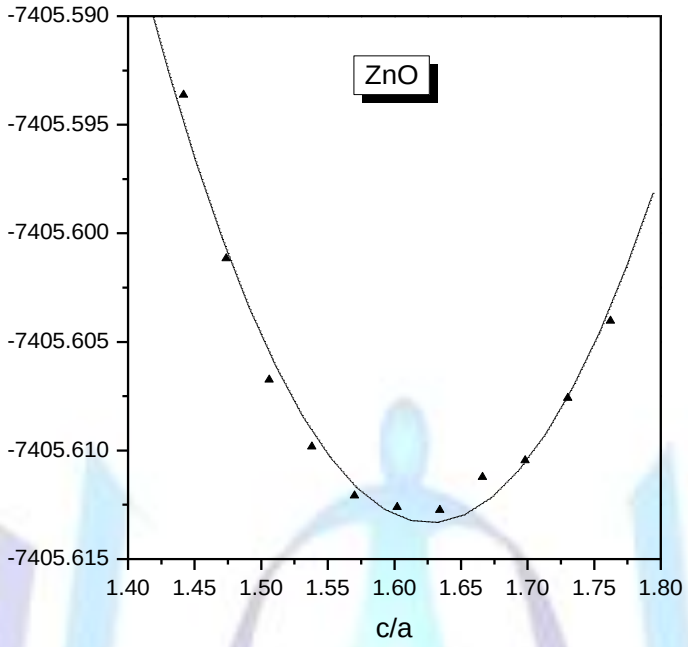

Figure 1b

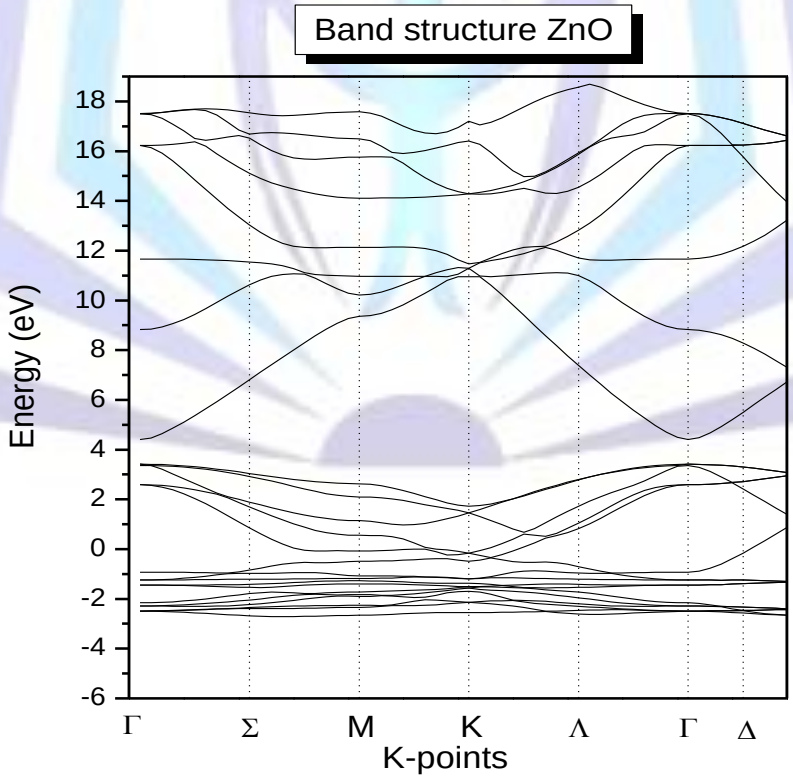

Figure 2

ISSN 2347-3487

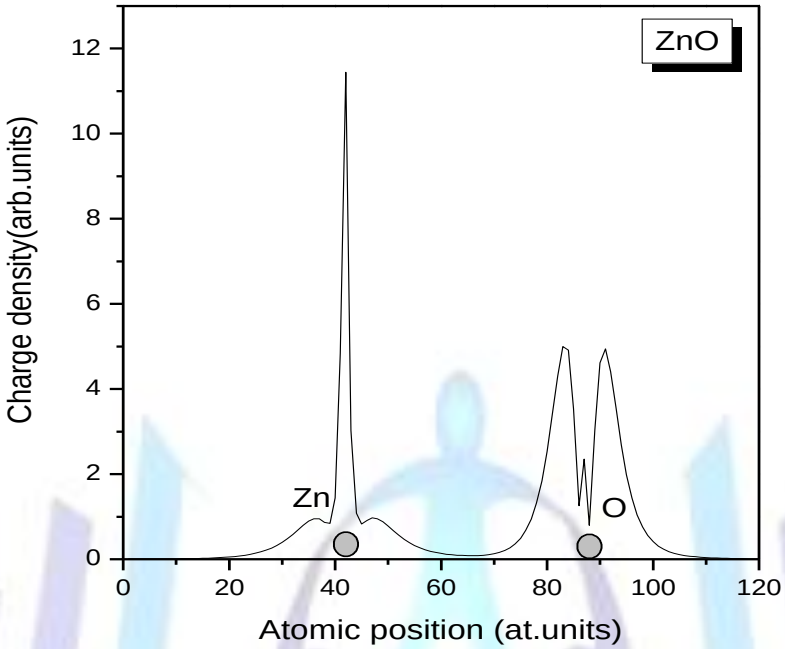

Figure 3a

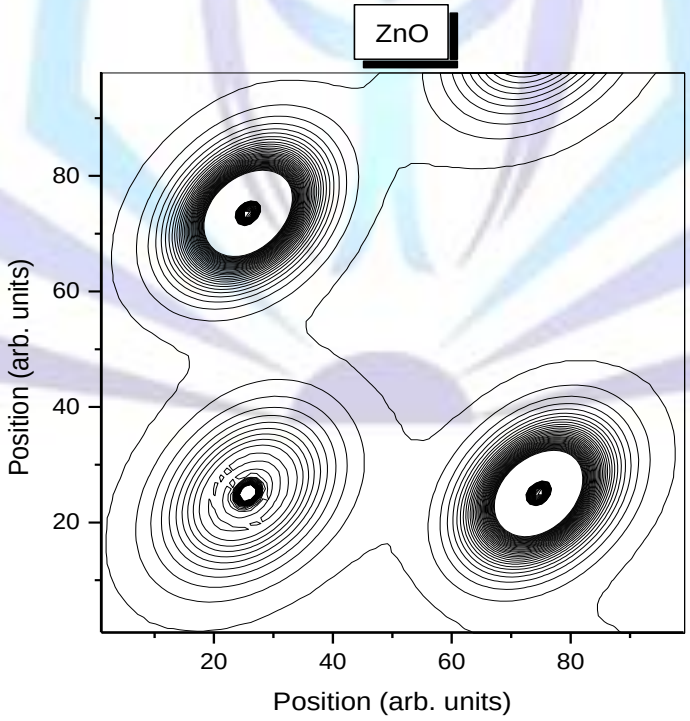

Figure 3b

ISSN 2347-3487

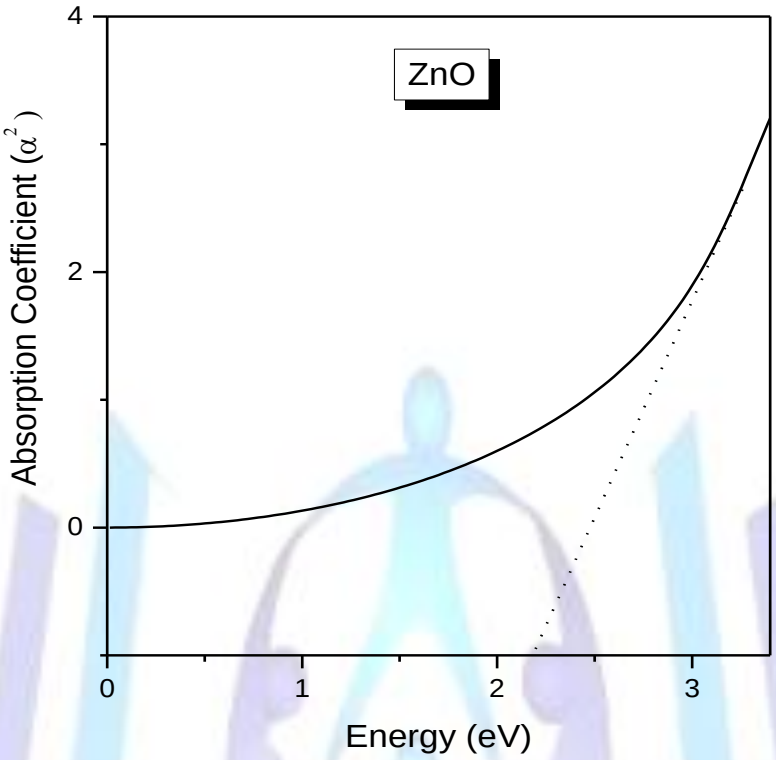

Figure 4

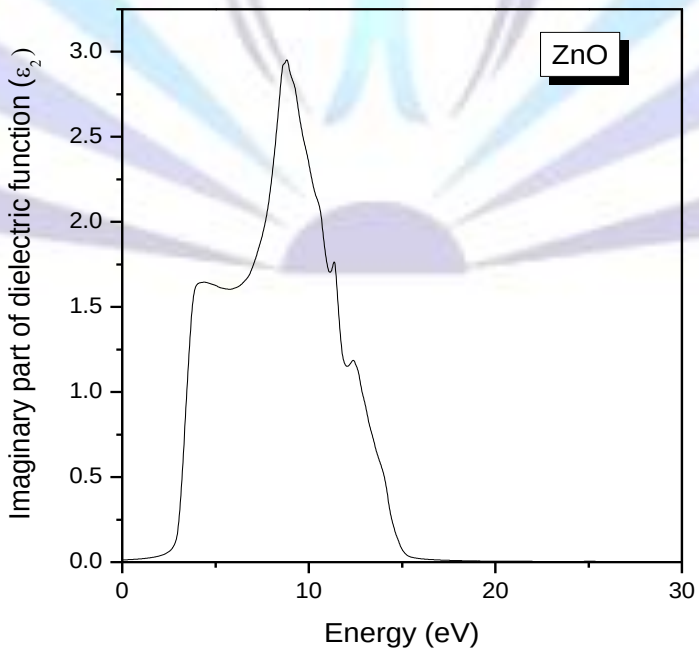

Figure 5a

ISSN 2347-3487

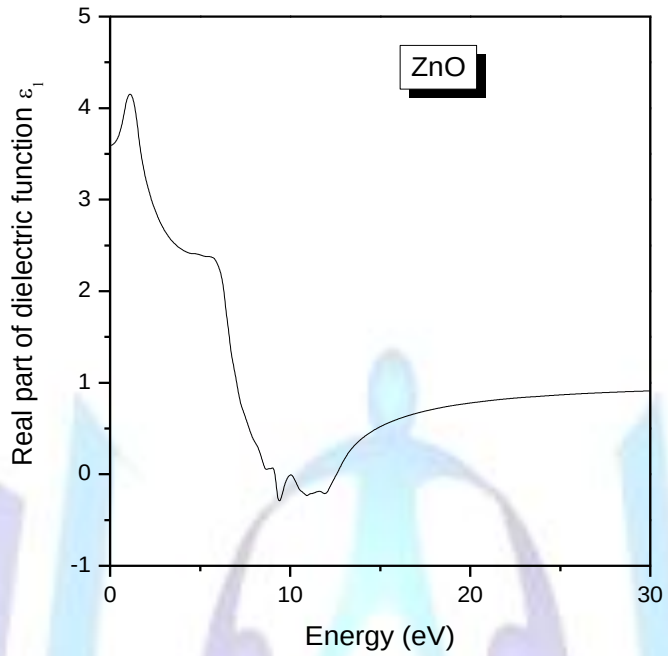

Figure 5b

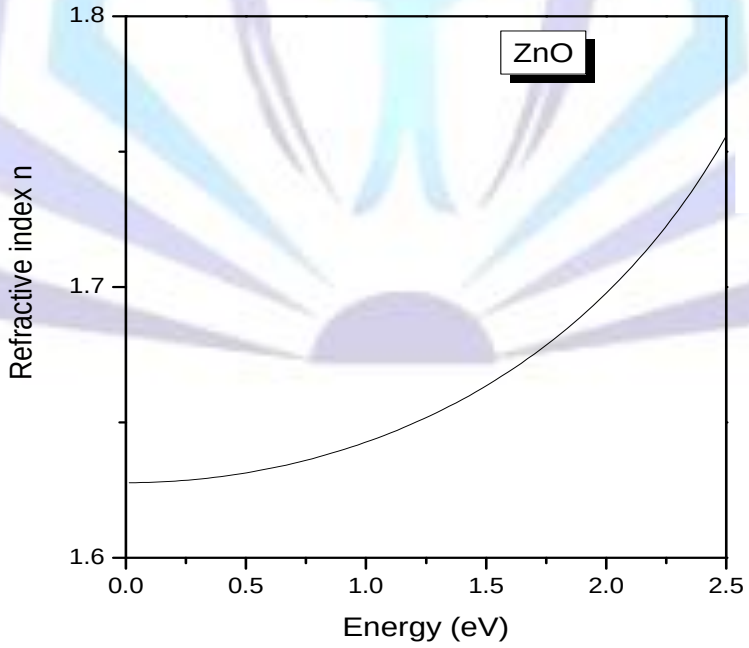

Figure 6

ISSN 2347-3487

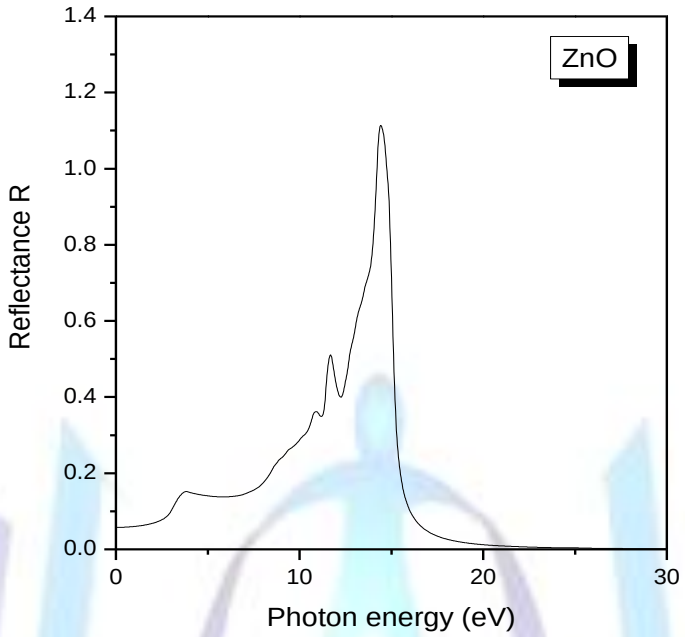

Figure 7